ADVANCED FUNCTIONAL MATERIALS
www.afm-journal.de

Materials Views
www.MaterialsViews.com

Photoluminescent Porous Si/SiO_2 Core/Shell Nanoparticles Prepared by Borate Oxidation

*Jinmyoung Joo, Jose F. Cruz, Sanahan Vijayakumar, Joel Grondek, and Michael J. Sailor**

A systematic study on the activation of photoluminescence from luminescent porous silicon nanoparticles (LPSiNPs) by oxidation in aqueous media containing sodium tetraborate (borax) is presented. The treatment promotes surface oxidation of the porous silicon skeleton and consequently generates an electronically passivated material. Photoluminescence is ascribed to quantum confinement effects and to defects localized at the Si-SiO_2 interface, and the strong photoluminescence is attributed to passivation of nonradiative surface defects. The oxidation treatment (carried out at 20 °C) generates a gradual blue shift of the photoluminescence peak wavelength (from 800 nm to 630 nm), while the bandwidth remains relatively constant (≈210 nm). During the treatment period, the external quantum yield (λ_{ex} = 365 nm) of photoluminescence increases to a maximum value of 23% after 200 min, and then it decreases at longer treatment times. The decrease in photoluminescence intensity at longer times is attributed to degradation and dissolution of the nanoparticles, which is inhibited at higher nanoparticle concentrations or by addition of free silicic acid.

1. Introduction

Since the discovery of room-temperature photoluminescence (PL) from electrochemically etched porous silicon (PSi),[1] luminescent silicon nanomaterials have been extensively studied for applications ranging from solid-state light emitting devices, to chemical sensing, to biological labeling.[2–4] As an indirect band-gap semiconductor, bulk silicon is an inefficient PL emitter, because slow electron-hole radiative recombination competes with nonradiative recombination at defect sites and through three-body Auger processes, leading to the low optical emission.[5] The emission from nanocrystalline silicon is much more efficient than the corresponding process in bulk silicon due to a combination of two effects: 1) electron and hole wave functions overlap more effectively in quantum-confined silicon,[6] and 2) nonradiative impurities and lattice defects are not as accessible when the bulk silicon material is divided into nanocrystalline domains.[5,7] It is widely accepted that the green to near infrared PL from PSi originates from band-to-band recombination of quantum-confined excitons,[8] and that the emissive centers responsible for PL are strongly influenced by oxides and other species at the Si surface.[9] This also appears to be the case for nanoparticles derived from PSi.

Micron-scale and nanoscale particles of luminescent PSi have been employed for biological applications due to their biocompatibility, biodegradability and large specific capacity for therapeutic reagents.[10–17] For in vivo imaging, luminescent PSi nanoparticles (LPSiNPs) are an attractive alternative to conventional heavy-metal-containing quantum dots, which have been shown to be toxic in biological environments.[18–21] In addition, the long-lived excited state of LPSiNPs allows high fidelity, low background imaging when employed in time gated experiments.[22] A limitation of LPSiNPs has been that the quantum yield is typically <10%,[10] significantly lower than direct band-gap semiconductor quantum dots or many of the common organic imaging fluorophores. For instance, with the proper surface passivation, CdSe and CdS quantum dots can achieve PL quantum yields of ≈80–90%.[23–26] A number of reports have demonstrated quantum yields for individual silicon nanocrystals as large as 60%,[27–32] however these are dense Si nanocrystals and not porous nanostructures. The relatively low quantum yield of LPSiNPs is assumed to be due to the existence of nonradiative defects at the surface of the high surface area silicon skeleton. A method for overcoming this specific limitation is needed.

Here we present a systematic study of the activation of photoluminescence in PSi derived nanoparticles by controlled chemical oxidation of the surface. A number of reports have demonstrated LPSiNPs as biological imaging agents,[4,10,22,33,34] and the material used in all of these can be considered to be a core-shell nanoparticle in which a shell of SiO_2 encases the active porous Si skeleton. However, the growth of oxide used to activate PL in these LPSiNPs has not been investigated in

Dr. J. Joo, J. Grondek, Prof. M. J. Sailor
Department of Chemistry and Biochemistry
University of California
San Diego 9500
Gilman Dr, La Jolla, CA 92093-0358, USA
E-mail: msailor@ucsd.edu
J. F. Cruz
Department of Chemical Engineering
University of California
San Diego 9500
Gilman Dr. La Jolla, CA 92093-0358, USA
S. Vijayakumar
Department of Mining and Materials Engineering
McGill University
Montreal, Quebec, Canada

DOI: 10.1002/adfm.201400587

detail. While it is evident that improvement of PL efficiency can be achieved through careful passivation of the nanocrystalline silicon surface, control of the chemistry of the passivation layer is crucial for a complete understanding of the luminescent properties and for the successful application of these materials in vivo. In particular, if the oxidation reaction proceeds too far, the Si core is completely eliminated and photoluminescence is destroyed. We previously found that mild oxidation with aqueous sodium tetraborate (borax) improves both quantum yield and stability of LPSiNPs.[35] It is shown here that the borax treatment can lead to quantum yields for LPSiNPs as high as 23% if the process is terminated at the appropriate point in the reaction.

2. Results and Discussion

The nanoparticles were prepared from highly doped p-type single-crystal silicon wafers using a three-step process. First, porous layers were etched into silicon by means of electrochemical etching in an aqueous electrolyte containing HF and ethanol. In order to control the size of the PSiNPs, high current pulses were applied periodically during an otherwise constant current etching process (**Figure 1**a).[14,36] The nominal pore diameter of the primary porous layer was ≈12 nm (Figure 1b), and the pores were preferentially oriented in the <100> direction, perpendicular to the surface of the wafer. The current pulses introduced thin layers of much higher porosity ("perforations") parallel to the <100> face of the wafer, which served as artificial cleavage planes to direct the fracture process into a size range determined by the physical spacing of the perforations. In a second step, the porous silicon layer was removed from the silicon substrate with a current pulse ("lift-off"). Finally, the free-standing porous Si layer was placed in deionized water and fractured by ultrasonication. The resulting PSiNPs showed very similar thickness along the pore axis, which corresponded to the thickness of the primary layers in the original films (Figure 1c). This process generated nanoparticles with consistent and reproducible dimensions and morphology. The hydrodynamic diameter measured by dynamic light scattering (200 ± 10 nm) was consistent with the TEM measurement (see Figure S1 in Supporting Information).

The typical means to activate PL in PSiNPs has been by incubation in deionized water at room temperature for 2 weeks.[10] During this activation step, a passivating silicon oxide layer grows on the hydrogen-terminated PSi surface. The resulting luminescent porous Si nanoparticles (LPSiNPs) display strong orange to near-infrared photoluminescence, which has been attributed to quantum confinement effects in the silicon cores and to localized Si-SiO_2 interfacial defects.[37–40] However, there are two competing chemical processes at work in the reaction of LPSiNPs with water. The first is the above-described growth of a surface oxide, which tends to increase photoluminescence intensity by passivation of electronic states on the nanoparticle surface. The second process is dissolution of this oxide. As the silicon oxide layer dissolves in the aqueous solution, fresh Si surface is exposed that can oxidize further. Taken to the limit, the entire particle will dissolve and photoluminescence will disappear. This dissolution step may be limited by the solubility of the silicic acid product, $Si(OH)_4$ or its rate of dissolution. We first studied this process by allowing LPSiNPs to oxidize in deionized water and measuring the temporal evolution of the PL spectrum as a function of concentration of nanoparticles. We hypothesized that under conditions of high [$Si(OH)_4$], nanoparticle dissolution would be inhibited. For these experiments the samples were covered to minimize water evaporation, although no effort was made to exclude oxygen from air. Initially, the as-prepared PSiNPs displayed very weak to undetectable photoluminescence under UV illumination, which increased gradually, coincident with the growth of a silicon oxide layer on the surface (see Figure S2 in Supporting Information). Photoluminescence intensity increased for a few hours to a few days, depending on the concentration of LPSiNPs. Samples with a larger concentration of nanoparticles required more time to reach maximum PL intensity. The measured PL intensity then decayed to the noise level within 5 to 30 days. Samples with a larger concentration of nanoparticles required more time to lose PL intensity. The loss of PL intensity at this stage of the experiment is attributed to the complete oxidation and dissolution of the nanoparticles, and it was confirmed by UV-Vis absorption (see Figure S3 in Supporting Information). The results indicate a strong dependence of oxidation/dissolution on particle concentration.

Because dissolution of $SiO_{2(s)}$ to form $Si(OH)_{4(aq)}$ is a reversible reaction, we suggest that the rate limiting step for the nanoparticle oxidation/dissolution process is the removal

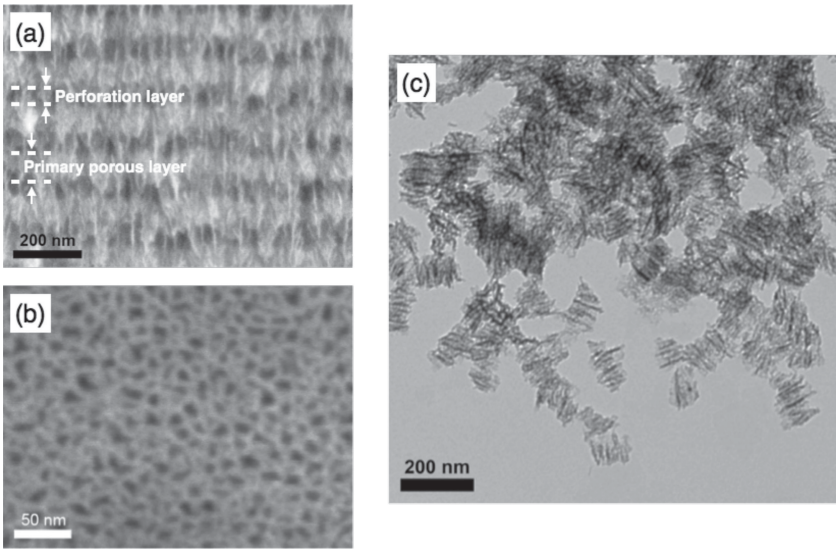

Figure 1. a,b) Scanning electron microscope (SEM) images of the PSi film before ultrasonication: The cross-sectional image (a) reveals the periodic perforation layers that act as artificial cleavage planes for nanoparticle formation, and the plan view (b) shows the pore dimensions. c) Transmission electron microscope (TEM) image of the PSiNPs formed after ultrasonication of the structure in (a,b).

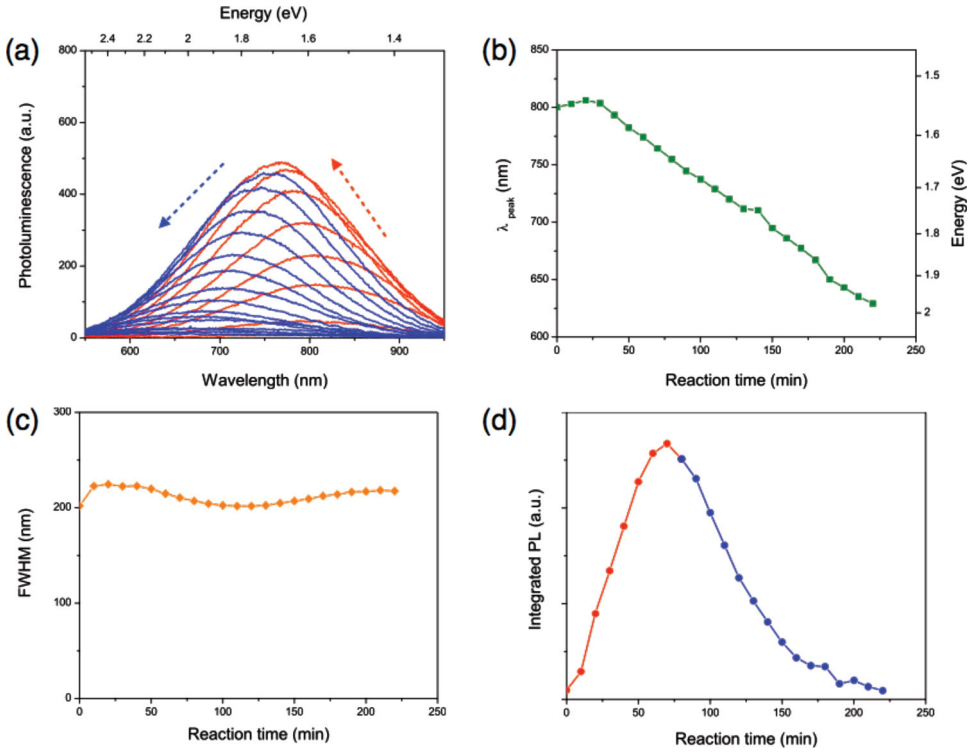

Figure 2. a) Photoluminescence emission spectra (λ_{ex}: 365 nm) of LPSiNPs (0.37 mg mL^{-1}) during reaction with 4.06 mM of aqueous sodium borate (Red: 0–70 min, Blue: 80–220 min). b) Corresponding PL peak wavelength shift, c) variance in FWHM, and d) integrated PL intensity as a function of reaction time. Red and blue color corresponds to curves shown in (a).

of surface oxide as dissolved $Si(OH)_{4(aq)}$, and that it proceeds more slowly as free $Si(OH)_{4(aq)}$ builds up in solution. To test this hypothesis, particle dissolution was studied as a function of concentration of free $Si(OH)_{4(aq)}$, added at the beginning of the experiment. The evolution of the PL spectrum shows a pronounced dependence on added $Si(OH)_{4(aq)}$ (Figure S4 in Supporting Information). Both the appearance and disappearance of photoluminescence occur on a slower time scale with increasing $[Si(OH)_{4(aq)}]$, indicating that it is the dissolution of the oxide shell, rather than oxidation of the silicon core, that is the rate limiting step. The oxidant in this case can be either water or dissolved oxygen.[41]

In order to increase the rate of silicon oxidation while at the same time minimizing the rate of oxide dissolution, we investigated the effect of aqueous sodium tetraborate (borax) on the reaction at room temperature. Borax is commonly used as a cleaner because it is a mild oxidant, it generates slightly basic solutions, and it can act as a buffer at pH ≈9.5.[42] **Figure 2**a shows PL spectra of LPSiNPs obtained at different time points during reaction with sodium tetraborate solution. We note three characteristics of the PL spectrum: 1) the peak wavelength shifts to the blue region (Figure 2b); 2) the peak bandwidth is broad throughout the process (Figure 2c); and 3) there is a gradual increase in intensity of PL followed by a decrease (Figure 2d). These characteristics are similar to what is observed with the pure water treatment, except in the case of aqueous tetraborate the reaction is much more rapid.

The observed blue shift in the PL spectrum with increasing reaction time is consistent with a decrease in size of the quantum-confined nanocrystalline silicon domains, as their outermost surface is converted from Si to SiO_2. Such behavior has been seen many times before, and it is a characteristic of air- or water-based oxidation of PSi surfaces.[9] The result of this chemical reaction is represented schematically in **Figure 3**: as-prepared PSiNPs have an H-terminated surface, with very little oxide initially. Oxidation removes these hydride species, and the underlying Si skeleton is gradually converted to SiO_2. With increasing oxidation time, the oxide layer grows thicker and the crystalline core becomes smaller. Consistent with the quantum confinement model of photoluminescence from PSi (radiative recombination of electron-hole pairs confined in crystalline silicon domains of <5nm in size), there is a corresponding blue shift in the PL spectrum with increasing extent of oxidation. The blue shift of the photoluminescence energy (E_{PL}, in eV) can be used to determine the change in the silicon core diameter d (in nm) based on the empirical inverse power law relationship of Equation (1):[32,43]

$$E_{PL} = E_g + \frac{3.73}{d^{1.39}} \quad (1)$$

where E_g is the band gap energy of crystalline Si (1.17 eV). **Figure 4** shows silicon crystallite sizes derived from this relationship as a function of oxidation time. It should be pointed out that the size determined here represents the size of the quantum-confined domains within a PSi nanoparticle, not the overall size of the PSi nanoparticle itself. This is consistent with DLS measurements obtained during tetraborate oxidation,

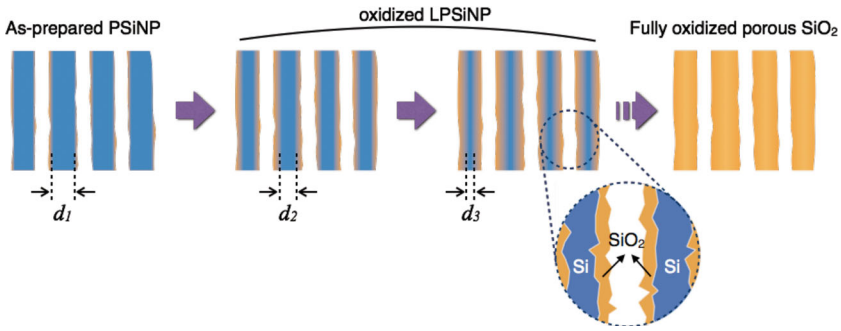

Figure 3. Schematic illustration depicting the oxidation of pore walls in a PSi sample. Blue represents silicon and orange is SiO_2. As the oxidation reaction progresses, the nanometer-scale Si features become smaller, leading to a blue shift in the quantum-confined photoluminescence spectrum. With more extensive oxidation, the Si domains disappear leaving a porous SiO_2 framework.

which show that the average particle size did not change substantially from ≈200 nm through the course of the 220 min reaction period (Figure S5 in Supporting Information). The calculated initial crystallite domain size is consistent with the nominal pore wall thickness (≈6 nm) of the PSi samples measured by SEM (Figure 1b), and the data indicate that the size of the silicon domains gradually decrease as a result of surface oxidation. The rate of crystallite size reduction, which induces the blue shift in the PL spectrum, is approximately constant over the course of the reaction except at the very beginning stage.

According to the estimate of eq. 1, the calculated average size of the silicon crystallites decreased to ≈3 nm by the end of the 220 min reaction period. There is a discrepancy between reported experimental values and theoretical estimates of Si crystallite size for diameters <3 nm,[44] so the estimates of crystallite size given in the present work should be considered approximate.

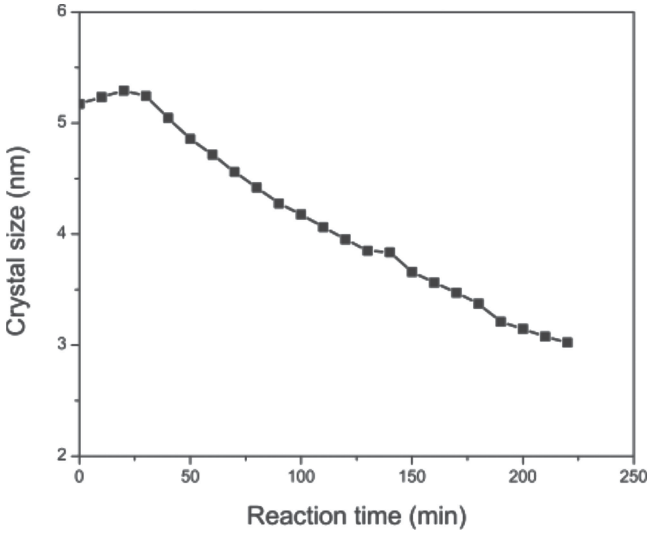

Figure 4. Calculated size of the quantum-confined domains in the LPSiNPs determined from the PL spectrum by equation (1) as a function of time during aqueous sodium tetraborate treatment. Sodium tetraborate concentration was 4.06 mM, LPSiNP concentration 0.37 mg mL^{-1}, reaction performed at room temperature.

The PL spectra shown in Figure 2a display single Gaussian profiles with a full width at half maximum (FWHM) of ≈200 nm for the entire reaction sequence (Figure 2c). The broad bandwidth is significantly larger than what is typical of CdSe quantum dots, for example, and it is consistent with the ensemble model of PSi, where the quantum-confined domains exist in a relatively broad distribution of sizes.[9] SEM measurements supported this interpretation; the PSi structures formed by electrochemical etching displayed a range of wall thicknesses (see Figure 1 and inset in Figure 3). The relatively constant FWHM that was observed throughout the reaction suggests that the nanocrystalline silicon walls were uniformly oxidized, resulting in a shrinking crystalline core within an oxide shell.

During the course of the 220 min oxidation reaction, the intensity of PL increased, reached a maximum, and then decreased to the point of being too weak to be observed (Figure 2d). The effect is too large to be attributable to the wavelength dependence of the instrument response, and it is believed to be primarily the result of an interplay between surface passivation by the growing oxide and nonradiative surface defects.

At the beginning of the oxidation process, the observed increase in PL intensity is ascribed to the passivation of nonradiative surface traps for electron-hole pairs. The highly reactive native hydride species and dangling bond states on the as-formed PSi surface are readily oxidized by mild oxidants.[41] Progressive oxidation of these and other nonradiative recombination centers is expected to generate a more passive oxide surface, increasing the PL intensity from nanocrystalline silicon.

Whereas the increase in PL intensity at the initial stage of the reaction is attributed to the passivation of active electronic defects, the decrease in PL intensity at longer reaction times is attributed to gradual shrinking and eventual elimination of quantum-confined Si domains. In addition, it is known that the radiative PL lifetime is much shorter for smaller Si nanocrystallites.[45] The observed decrease in PL intensity as the nanoparticles approach 3 nm in diameter is consistent with a prior report, which indicated that the PL intensity of very small (<2.5nm) Si nanocrystals is low due to the development of oxide-related surface states within the band gap of the nanocrystals.[8] Thus, while oxide passivation of the outmost surface can increase PL intensity from nanocrystalline Si by eliminating more active surface defects on the larger nanoparticles, as the nanoparticles reach smaller sizes the oxide itself can become more defective and less passivating. The later stages of oxide growth are therefore expected to result in a decrease in PL due to increasing incidence of nonradiative defect centers. Of course the continued growth of oxide will lead to elimination of the crystalline Si chromophore altogether, and this is also expected to contribute to the decrease in observed PL intensity at the latter stage of the oxidation reaction. It should be pointed out that the oscillator strength of the LPSiNPs is expected to decrease with

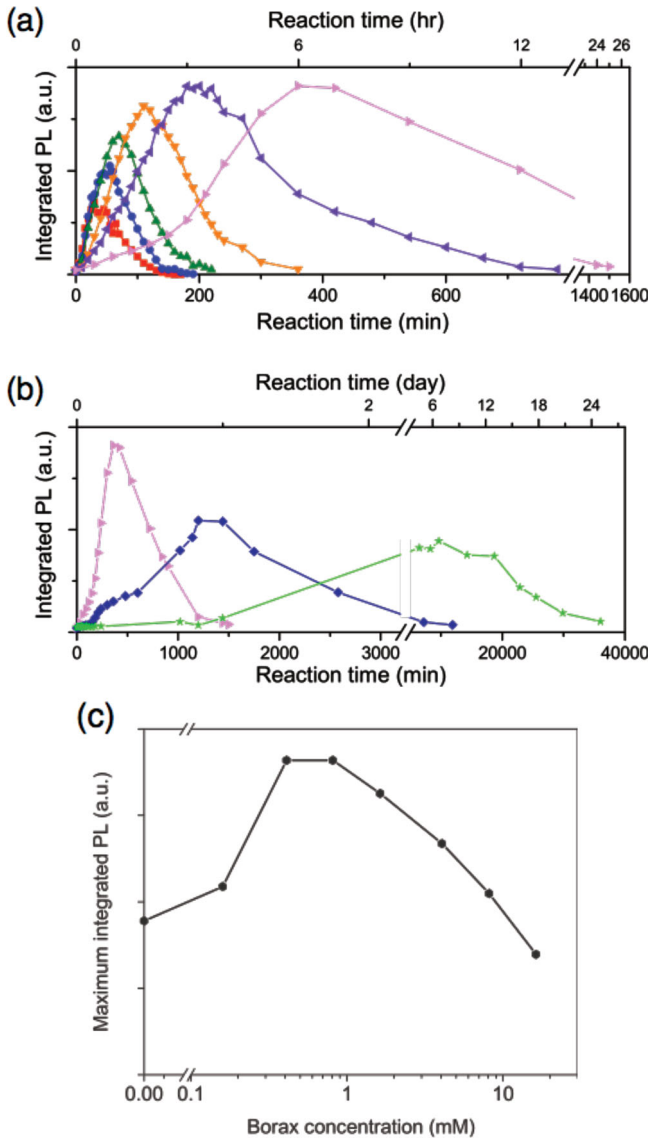

Figure 5. a,b) Integrated intensity of PL (λ_{em} from 550 nm to 980 nm) of LPSiNPs (0.37 mg mL^{-1}) allowed to react with different concentrations of aqueous sodium tetraborate as a function of reaction time: a) Reaction time 0–1600 min. Sodium tetraborate concentrations (for the indicated traces): 16.26 mM (red squares, ■ □), 8.13 mM (blue circles, ●), 4.06 mM (green up triangles, ▲), 1.63 mM (orange down triangles, ▼), 0.81 mM (violet left triangles, ◀ □), 0.41 mM (pink right triangles, ▶). b) Reaction time 0–40,000 min: 0.41 mM (pink right triangles, ▶), 0.16 mM (dark blue diamonds, ◆), pure H_2O control with no sodium tetraborate (light green stars, ★). c) Maximum integrated PL intensity from the traces in plots (a) and (b), as a function of sodium tetraborate concentration.

size too, and so defect passivation/generation represents only an approximate picture.

The results provide additional support to the "vibron" model, in which quantum-confined electronic states in the Si nanocrystals are resonantly coupled to Si-O vibrations at the nanocrystal interface, leading to high PL efficiency.[9] It has been experimentally demonstrated that the energy difference between the lowest valence sublevels in Si nanocrystals becomes comparable to the energy difference between Si-O surface vibrations for nanocrystals in the size range of 4–4.5 nm, and so resonant coupling should be most pronounced in this size range. Our experimental finding is in good agreement with the model, because the PL intensity reaches a maximum 70 min after initiation of the reaction, at which point the calculated Si crystallite size is 4.5 nm (Figure 2b and Figure 4). The main conclusion from this study is that PL intensity from LPSiNPs is a trade-off between surface passivation, defect generation, chemical reaction rates, and other photophysical properties related to the oxidation process and the energy level in the nanocrystallites. For the aqueous tetraborate oxidant system, those parameters combine to yield a maximum in PL intensity at a specific point in time during oxidation.

The point in time at which the PL intensity reaches a maximum strongly depends on tetraborate concentration. **Figure 5** shows the integrated PL intensity of a fixed concentration of LPSiNPs allowed to react with solutions of different tetraborate concentrations. For all concentrations of tetraborate, the PL spectrum blue shifted as the intensity gradually increased and then decreased (see also Figure S6 in Supporting Information). The more rapid increase in PL was observed at higher tetraborate concentrations, and this is attributed to a faster rate of oxidation. The maximum PL intensities corresponding to the data of Figure 5a and b are shown in Figure 5c as a function of tetraborate concentration. As discussed above, a similar blue shift and variation in integrated PL intensity was obtained in the reaction with deionized water, although reaction of LPSiNPs with deionized water containing no tetraborate resulted in the slowest observed rate of oxidation and a lower maximum in PL intensity relative to reactions with tetraborate-containing solutions (Figure 5b,c and Figure S6 in Supporting Information). Interestingly, intermediate tetraborate concentrations of 0.8 mM showed the greatest maximum in PL intensity. Using rhodamine 6G as a standard, the optimum quantum yield (QY) of the LPSiNPs was found to be 23.1%, for samples oxidized in 0.81 mM tetraborate for 200 min at room temperature. This is the largest quantum yield for LPSiNPs reported to date. As mentioned above, it is known that the formation of a native oxide layer on the Si surface can lead to an increase in the PL intensity because the oxide passivates nonradiative surface defects. However, it is likely that the oxide layer formed at higher tetraborate concentrations does not sufficiently passivate the defects due to the high rate of the reaction. On the other hand, the smaller maximum PL intensity observed for the samples measured at lower tetraborate concentrations and in tetraborate-free deionized water presumably result from too rapid dissolution of the passivating silicon oxide.[41] From these results, we conclude that it is important to control both the rate of oxidation and the rate of oxide dissolution to maximize PL from LPSiNPs.

Aqueous stability of the LPSiNPs is a key issue for long-term in vivo drug delivery and bioimaging applications. Importantly, the tetraborate treatment also resulted in a considerable increase in the aqueous stability of LPSiNPs. Stability of the LPSiNPs was tested by incubation in aqueous phosphate buffered saline (PBS) of physiological pH and ionic strength at 37 °C. Samples of LPSiNPs prepared using the optimized tetraborate treatment were compared with LPSiNPs prepared via the previously reported 2-week oxidation in deionized water.

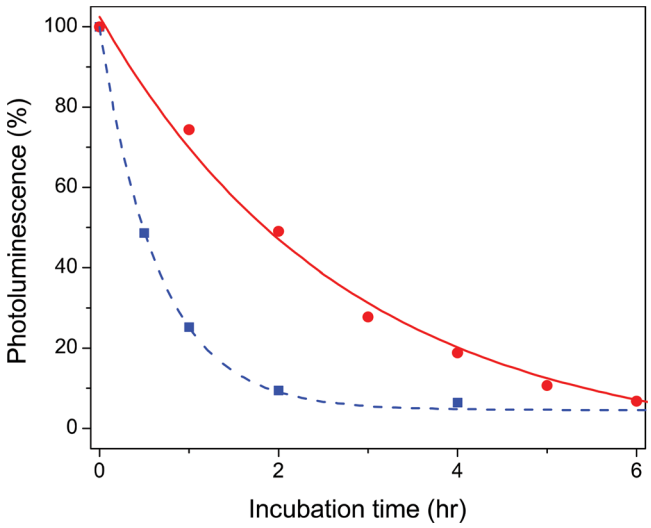

Figure 6. Integrated PL intensity (λ_{ex}: 365 nm, λ_{em}: 550–980 nm) from a sample of LPSiNPs (50 μg mL^{-1}) incubated in PBS solution at 37 °C as a function of time. Blue dashed trace: LPSiNPs oxidized in deionized water (QY ≈ 9.8%), Red solid trace: tetraborate-oxidized LPSiNPs (QY ≈23.1%)).

Stability was assessed by measurement of the spectrally integrated PL emission intensities as a function of time (**Figure 6**). The tetraborate-free, water-oxidized LPSiNPs (QY ≈9.8%) lost 50% of their original PL intensity in 30 min, consistent with a previous report.[10] The tetraborate-oxidized LPSiNPs (QY ≈23.1%) showed slower degradation kinetics, losing 50% of their original PL intensity in 2 h. Thus the tetraborate oxidation method provides material with 2× greater quantum yield and 4× longer residence time at physiologic pH and temperature than the water oxidation method.

3. Conclusion

Aqueous sodium tetraborate solutions provide a mild and rapid (2 hr) means to prepare Si/SiO_2 core/shell nanoparticles from porous Si nanoparticles. Systematic optimization of reaction conditions provided a material with greater stability in aqueous PBS solutions (2 hours) and larger photoluminescence quantum yield of 23% (λ_{ex}: 365 nm) than material made via oxidation in pure water. During the aqueous oxidation in tetraborate, the wavelength of maximum PL shifts to higher energy while the spectral bandwidth remains approximately constant (at 200 nm FWHM) with time. The PL intensity is observed to gradually increase, reach a maximum, and then decrease. The time course of this process depends on the concentration of nanoparticles, the concentration of free silicic acid, and on the concentration of borate, and is interpreted as a trade-off between oxidation of the Si core and dissolution of the SiO_2 shell.

4. Experimental Section

Materials: Silicon wafers (≈1 mΩ cm resistivity, <100> orientation) were obtained from Virginia Semiconductor, Inc. Sodium tetraborate decahydrate, silicic acid and rhodamine 6G ware purchased from Sigma-Aldrich Chemicals. Phosphate buffered saline (PBS, 1×, Gibco, pH 7.4) without Mg^{2+} and Ca^{2+} was obtained from Life Technologies. All chemicals were used without further purification.

Preparation of Luminescent Porous Silicon Nanoparticles (LPSiNPs): Porous silicon films were prepared by electrochemical etch of highly boron-doped p^{++}-type single-crystal silicon wafers in an electrolyte consisting of 3:1 (by volume) of 48% aqueous HF:ethanol. The etching waveform consisted of a square wave in which a lower value of current density of 50 mA cm^{-2} was applied for 1.8 sec, followed by a higher value of current density of 400 mA cm^{-2} for 0.36 sec. This waveform was repeated for 140 cycles, generating a perforated PSi film with alternating layers of high and low porosity.[14,36] The etched porous nanostructure was removed from the Si substrate by application of a current pulse of 3.7 mA cm^{-2} for 250 sec in a solution of 1:29 (by volume) of 48% aqueous HF:ethanol. The freestanding PSi film was fractured by ultrasonication (50T, VWR International) overnight, and the resulting colloidal dispersion of PSi nanoparticles was used without filtration. The PSiNPs (0.37 mg/ml) were then immersed in aqueous solutions of sodium tetraborate of various concentrations (0–16.26 mM) to activate photoluminescence, and PL spectra of the resulting LPSiNPs were monitored at each time point.

Characterization: Scanning electron microscope (SEM) images were obtained with an FEI XL30 field-emission instrument operating in secondary electron imaging mode. Transmission electron microscope (TEM) images were obtained on a JEOL-1200 EX II instrument operating at 120 kV. Dynamic light scattering (DLS, Zetasizer ZS90, Malvern Instruments) was used to determine the hydrodynamic size of the nanoparticles. The PL spectra (λ_{ex}: 365 nm) were obtained using Ocean Optics QE-65 spectrometer with 460 nm long-pass emission filter. The quantum yield (QY) of LPSiNPs in ethanol was measured using the comparative method, using Rhodamine 6G in ethanol as a standard.[46] A series of solutions of Rhodamine 6G or LPSiNPs were prepared with concentrations adjusted such that the optical absorbance values were between 0 – 0.1 at 365 nm. The PL spectra were measured (λ_{ex} = 365 nm) and the PL intensity was integrated between the wavelength values 500–980 nm. Quantum yields were determined by comparison of the integrated PL intensity vs absorbance curves (Figure S7 in the Supporting Information), assuming QY of 95% for the Rhodamine 6G standard.

Supporting Information

Supporting Information is available from the Wiley Online Library or from the author.

Acknowledgements

This work supported by the National Science Foundation under Grant No. DMR-1210417 and by the Defense Advanced Research Projects Agency (DARPA) under Cooperative Agreement HR0011–13–2–0017. The content of the information within this document does not necessarily reflect the position or the policy of the Government.

Received: February 19, 2014
Revised: April 13, 2014
Published online: July 9, 2014

[1] L. T. Canham, *Appl. Phys. Lett.* **1990**, *57*, 1046.
[2] R. J. Walters, G. I. Bourianoff, H. A. Atwater, *Nat. Mater.* **2005**, *4*, 143.
[3] M. J. Sailor, E. C. Wu, *Adv. Funct. Mater.* **2009**, *19*, 3195.
[4] Z. F. Li, E. Ruckenstein, *Nano Lett.* **2004**, *4*, 1463.

[5] L. E. Brus, P. F. Szajowski, W. L. Wilson, T. D. Harris, S. Schuppler, P. H. Citrin, *J. Am. Chem. Soc.* **1995**, *117*, 2915.
[6] C. Delerue, G. Allan, M. Lannoo, *Phys. Rev. B* **2001**, *64*, 193402.
[7] R. J. Walters, J. Kalkman, A. Polman, H. A. Atwater, M. J. A. de Dood, *Phys. Rev. B* **2006**, *73*, 132302.
[8] M. V. Wolkin, J. Jorne, P. M. Fauchet, G. Allan, C. Delerue, *Phys. Rev. Lett.* **1999**, *82*, 197.
[9] A. Sa'ar, *J Nanophotonics* **2009**, *3*, 032501.
[10] J. H. Park, L. Gu, G. von Maltzahn, E. Ruoslahti, S. N. Bhatia, M. J. Sailor, *Nat. Mater.* **2009**, *8*, 331.
[11] S. C. Bayliss, R. Heald, D. I. Fletcher, L. D. Buckberry, *Adv. Mater.* **1999**, *11*, 318.
[12] L. T. Canham, *Adv. Mater.* **1995**, *7*, 1033.
[13] E. Tasciotti, X. W. Liu, R. Bhavane, K. Plant, A. D. Leonard, B. K. Price, M. M. C. Cheng, P. Decuzzi, J. M. Tour, F. Robertson, M. Ferrari, *Nat. Nanotechnol.* **2008**, *3*, 151.
[14] L. M. Bimbo, M. Sarparanta, H. A. Santos, A. J. Airaksinen, E. Makila, T. Laaksonen, L. Peltonen, V. P. Lehto, J. Hirvonen, J. Salonen, *ACS Nano* **2010**, *4*, 3023.
[15] F. Erogbogbo, K. T. Yong, I. Roy, G. X. Xu, P. N. Prasad, M. T. Swihart, *ACS Nano* **2008**, *2*, 873.
[16] S. P. Low, N. H. Voelcker, L. T. Canham, K. A. Williams, *Biomaterials* **2009**, *30*, 2873.
[17] D. M. Fan, E. De Rosa, M. B. Murphy, Y. Peng, C. A. Smid, C. Chiappini, X. W. Liu, P. Simmons, B. K. Weiner, M. Ferrari, E. Tasciotti, *Adv. Funct. Mater.* **2012**, *22*, 282.
[18] A. M. Derfus, W. C. W. Chan, S. N. Bhatia, *Nano Lett.* **2004**, *4*, 11.
[19] N. H. Cho, T. C. Cheong, J. H. Min, J. H. Wu, S. J. Lee, D. Kim, J. S. Yang, S. Kim, Y. K. Kim, S. Y. Seong, *Nat. Nanotechnol.* **2011**, *6*, 675.
[20] T. S. Hauck, R. E. Anderson, H. C. Fischer, S. Newbigging, W. C. W. Chan, *Small* **2010**, *6*, 138.
[21] H. S. Choi, W. Liu, P. Misra, E. Tanaka, J. P. Zimmer, B. I. Ipe, M. G. Bawendi, J. V. Frangioni, *Nat. Biotechnol.* **2007**, *25*, 1165.
[22] L. Gu, D. J. Hall, Z. Qin, E. Anglin, J. Joo, D. J. Mooney, S. B. Howell, M. J. Sailor, *Nat. Commun.* **2013**, *4*, 2326.
[23] D. V. Talapin, I. Mekis, S. Gotzinger, A. Kornowski, O. Benson, H. Weller, *J. Phys. Chem. B* **2004**, *108*, 18826.
[24] P. Reiss, J. Bleuse, A. Pron, *Nano Lett.* **2002**, *2*, 781.
[25] I. Mekis, D. V. Talapin, A. Kornowski, M. Haase, H. Weller, *J. Phys. Chem. B* **2003**, *107*, 7454.
[26] A. B. Greytak, P. M. Allen, W. H. Liu, J. Zhao, E. R. Young, Z. Popovic, B. J. Walker, D. G. Nocera, M. G. Bawendi, *Chem Sci* **2012**, *3*, 2028.
[27] D. Timmerman, J. Valenta, K. Dohnalova, W. D. A. M. de Boer, T. Gregorkiewicz, *Nat. Nanotechnol.* **2011**, *6*, 710.
[28] M. L. Mastronardi, F. Maier-Flaig, D. Faulkner, E. J. Henderson, C. Kubel, U. Lemmer, G. A. Ozin, *Nano Lett.* **2012**, *12*, 337.
[29] R. J. Anthony, D. J. Rowe, M. Stein, J. H. Yang, U. Kortshagen, *Adv. Funct. Mater.* **2011**, *21*, 4042.
[30] R. Anthony, U. Kortshagen, *Phys. Rev. B* **2009**, *80*, 115407.
[31] D. Jurbergs, E. Rogojina, L. Mangolini, U. Kortshagen, *Appl. Phys. Lett.* **2006**, *88*, 233116.
[32] G. Ledoux, O. Guillois, D. Porterat, C. Reynaud, F. Huisken, B. Kohn, V. Paillard, *Phys. Rev. B* **2000**, *62*, 15942.
[33] F. Erogbogbo, K. T. Yong, I. Roy, R. Hu, W. C. Law, W. W. Zhao, H. Ding, F. Wu, R. Kumar, M. T. Swihart, P. N. Prasad, *ACS Nano* **2011**, *5*, 413.
[34] C. M. Hessel, M. R. Rasch, J. L. Hueso, B. W. Goodfellow, V. A. Akhavan, P. Puvanakrishnan, J. W. Tunnel, B. A. Korgel, *Small* **2010**, *6*, 2026.
[35] L. Gu, J. H. Park, K. H. Duong, E. Ruoslahti, M. J. Sailor, *Small* **2010**, *6*, 2546.
[36] Z. Qin, J. Joo, L. Gu, M. J. Sailor, *Part. Part. Syst. Char.* **2014**, *31*, 252.
[37] J. L. Heinrich, C. L. Curtis, G. M. Credo, K. L. Kavanagh, M. J. Sailor, *Science* **1992**, *255*, 66.
[38] W. L. Wilson, P. F. Szajowski, L. E. Brus, *Science* **1993**, *262*, 1242.
[39] S. Godefroo, M. Hayne, M. Jivanescu, A. Stesmans, M. Zacharias, O. I. Lebedev, G. Van Tendeloo, V. V. Moshchalkov, *Nat. Nanotechnol.* **2008**, *3*, 174.
[40] E. Froner, R. Adamo, Z. Gaburro, B. Margesin, L. Pavesi, A. Rigo, M. Scarpa, *J. Nanopart. Res.* **2006**, *8*, 1071.
[41] M. J. Sailor, *Porous Silicon in Practice Preparation, Characterization and Applications*, Wiley-VCH, Weinheim, Germany, **2012**.
[42] W.-P. Leung, Q. W.-Y. Ip, in *Encyclopedia of Inorganic Chemistry*, 2nd ed. (Eds.: R. B. King), Wiley, Chichester; Hoboken, NJ, **2006**, p. 10.
[43] C. Delerue, G. Allan, M. Lannoo, *Phys. Rev. B* **1993**, *48*, 11024.
[44] G. Ledoux, J. Gong, F. Huisken, O. Guillois, C. Reynaud, *Appl. Phys. Lett.* **2002**, *80*, 4834.
[45] A. G. Cullis, L. T. Canham, P. D. J. Calcott, *J. Appl. Phys.* **1997**, *82*, 909.
[46] R. F. Kubin, A. N. Fletcher, *J. Lumin.* **1982**, *27*, 455.